MAGNETIC NEUTRON SCATTERING

JEFFREY W. LYNN

NIST Center for Neutron Research, National Institute of Standards and Technology, Gaithersburg, Maryland

INTRODUCTION

The neutron is a spin-$^1/_2$ particle that carries a magnetic dipole moment of -1.913 nuclear magnetons. Magnetic neutron scattering then originates from the interaction of the neutron's spin with the unpaired electrons in the sample, either through the dipole moment associated with an electron's spin or via the orbital motion of the electron. The strength of this magnetic dipole–dipole interaction is comparable to the neutron–nuclear interaction, and thus there are magnetic cross-sections that are analogous to the nuclear ones that reveal the structure and dynamics of materials over wide ranges of length scale and energy. Magnetic neutron scattering plays a central role in determining and understanding the microscopic properties of a vast variety of magnetic systems, from the fundamental nature, symmetry, and dynamics of magnetically ordered materials to elucidating the magnetic characteristics essential in technological applications.

One traditional role of magnetic neutron scattering has been the measurement of magnetic Bragg intensities in the magnetically ordered regime. Such measurements can be used to determine the spatial arrangement and directions of the atomic magnetic moments, the atomic magnetization density of the individual atoms in the material, and the value of the ordered moments as a function of thermodynamic parameters such as temperature, pressure, and applied magnetic field. These types of measurements can be carried out on single crystals, powders, thin films, and artificially grown multilayers, and often the information collected can be obtained by no other experimental technique. For magnetic phenomena that occur over length scales that are large compared to atomic distances, the technique of magnetic small-angle neutron scattering (SANS) can be applied, in analogy to structural SANS. This is an ideal technique to explore domain structures, long-wavelength oscillatory magnetic states, vortex structures in superconductors, and other spatial variations of the magnetization density on length scales from 1 to 1000 nm. Another specialized technique is neutron reflectometry, which can be used to investigate the magnetization profile in the near-surface regime of single crystals, as well as the magnetization density of thin films and multilayers, in analogy with structural reflectometry techniques. This particular neutron technique has enjoyed remarkable growth over the last few decades due to the dramatic advancements in atomic deposition capabilities.

Neutrons can also scatter inelastically, to reveal the magnetic fluctuation spectrum of a material over wide ranges of energy (from $\sim 10^{-8}$ to 1 eV) and over the entire Brillouin zone. Neutron scattering plays a truly unique role in that it is the only technique that can directly determine the complete magnetic excitation spectrum, whether it is in the form of the dispersion relations for spin-wave excitations, wave vector and energy dependence of critical fluctuations, crystal field excitations, magnetic excitons, or moment fluctuations. In the present overview we will discuss some of these possibilities.

Competitive and Related Techniques

Much of the information that can be obtained from neutron scattering, such as ordering temperatures, critical parameters, and ferromagnetic moments, can and should be compared with magnetic measurements of quantities such as specific heat, susceptibility, and magnetization (Chapter 6). Indeed it is often highly desirable to have measurements available from these traditional techniques before undertaking the neutron measurements, as a way of both characterizing the particular specimen being investigated and being able to focus the neutron data collection to the range of temperature, applied field, etc., of central interest. Accordingly these complementary measurements are highly desirable.

For magnetic diffraction, the technique that is directly competitive is magnetic x-ray scattering. The x-ray magnetic cross-sections are typically $\sim 10^{-6}$ of those of charge scattering, but with the high fluxes available from synchrotron sources these cross-sections are readily observable. The information that can be obtained is also complementary to neutrons in that neutrons scatter from the total magnetization in the system, whether it originates from spin or orbital momenta, while for x-rays the spin and orbital contributions can be distinguished. X-rays also have the advantage that the wavelength can be tuned to an electronic resonance, which can increase the cross-section by as much as $\sim 10^4$, and thus it can be an element-specific technique. However, the limited number of resonances available restricts the materials that can be investigated, while the high absorption cross-sections and the generally more stringent experimental needs and specimen requirements are disadvantages. Each x-ray photon also carries $\sim 10^6$ times the energy that a neutron carries, and the combination of this with the brightness of a synchrotron source can cause rather dramatic changes in the physical or chemical properties of the sample during the investigation. Neutrons are a much gentler probe, but the low flux relative to synchrotron sources also means that larger samples are generally needed. Both techniques must be carried out at centralized facilities. Magnetic x-ray diffraction is a newer technique but has become more common as the technique has developed and matured. However, neutron scattering generally continues to be the technique of choice when investigating new materials.

For the investigation of spin dynamics, there are a number of experimental techniques that can provide important information. Mössbauer spectroscopy (9c.1), muon precession, and perturbed angular correlation measurements can reveal characteristic timescales, as well as information about the site symmetry of the

Characterization of Materials, edited by Elton N. Kaufmann.

magnetism and the ordered moment as a function of temperature. Raman and infrared spectroscopy can reveal information about the long-wavelength (Brillouin zone center) excitations, and the magnon density of states via two-magnon processes. Microwave absorption can determine the spin-wave excitation spectrum at very long wavelengths (small wave vectors $\mathbf{q}$), while nuclear magnetic resonance (9a.1) can give important information about relaxation rates. However, none of these techniques can explore the full range of dynamics that neutrons can, and in this regard there is no competitive experimental technique for measurements of the spin dynamics.

PRINCIPLES OF THE METHOD

Magnetic Diffraction

The cross-section for magnetic Bragg scattering is given by (Bacon, 1975)

$$I_{\mathrm{M}}(\tau) = C\left(\frac{\gamma e^2}{2mc^2}\right)^2 M_\tau A(\theta_{\mathrm{B}})|F_{\mathrm{M}}(\tau)|^2 \qquad (1)$$

where I_{M} is the integrated intensity for the magnetic Bragg reflection located at the reciprocal lattice vector $\boldsymbol{\tau}$, the neutron–electron coupling constant in parentheses is -0.27×10^{-12} cm, C is an instrumental constant that includes the resolution of the measurement, $A(\theta_{\mathrm{B}})$ is an angular factor that depends on the method of measurement (sample angular rotation, θ:2θ scan, etc.), and M_τ is the multiplicity of the reflection (for a powder sample). The magnetic structure factor $F_{\mathrm{M}}(\boldsymbol{\tau})$ is given in the general case by (Blume, 1961)

$$F_{\mathrm{M}}(\boldsymbol{\tau}) = \sum_{j=1}^{N} \mathrm{e}^{\mathrm{i}\boldsymbol{\tau}\cdot\mathbf{r}_j}\, \hat{\boldsymbol{\tau}} \times \left[\mathbf{M}_j(\boldsymbol{\tau}) \times \hat{\boldsymbol{\tau}}\right] \mathrm{e}^{-W_j} \qquad (2)$$

where $\hat{\boldsymbol{\tau}}$ is a unit vector in the direction of the reciprocal lattice vector $\boldsymbol{\tau}$, $\mathbf{M}_j(\tau)$ is the vector form factor of the jth ion located at $\mathbf{r}_j$ in the unit cell, W_j is the Debye–Waller factor (see unit 9c.1) that accounts for the thermal vibrations of the jth ion, and the sum is over all (magnetic) atoms in the unit cell. The triple cross-product originates from the vector nature of the dipole–dipole interaction of the neutron with the electron. A quantitative calculation of $\mathbf{M}_j(\boldsymbol{\tau})$ in the general case involves evaluating matrix elements of the form $\langle \pm | 2S\, \mathrm{e}^{\mathrm{i}\boldsymbol{\tau}\cdot\mathbf{R}} + O | \pm \rangle$, where S is the (magnetic) spin operator, O is the symmetrized orbital operator introduced by Trammell (1953), and $|\pm\rangle$ represents the angular momentum state. This can be quite a complicated angular momentum computation involving all the electron orbitals in the unit cell. However, often the atomic spin density is *collinear*, by which we mean that at each point in the spatial extent of the electron's probability distribution, the *direction* of the atomic magnetization density is the same. In this case the direction of $\mathbf{M}_j(\boldsymbol{\tau})$ does not depend on τ, and the form factor is just a scalar function, $f(\boldsymbol{\tau})$, which is simply related to the Fourier transform of the magnetization density. The free-ion form factors have been tabulated for essentially all the elements. If you are familiar with x-ray diffraction, then it is helpful to note that the magnetic form factor for neutron scattering is analogous to the form factor for charge scattering of x-rays, except that for x-rays it corresponds to the Fourier transform of the *total charge density* of all the electrons, while in the magnetic neutron case it is the transform of the "magnetic" electrons, which are the electrons whose spins are unpaired. Recalling that a Fourier transform inverts the relative size of objects, the magnetic form factor typically decreases more rapidly with $\boldsymbol{\tau}$ than for the case of x-ray charge scattering, since the unpaired electrons are usually the outermost ones of the ion. This dependence of the scattering intensity on $f(\boldsymbol{\tau})$ is a convenient way to distinguish magnetic cross-sections from the neutron scattering via nuclear cross-sections, where the equivalent of the magnetic form factor is just a constant (the nuclear coherent scattering amplitude b).

If the magnetic system is sufficiently simple, the correct magnetic structure can be obtained by inspection, but the more complicated magnetic materials that typically are currently under investigation can have quite a number of magnetic ions in the magnetic unit cell, and group theory is often helpful in elucidating the possible allowed magnetic configurations allowed by symmetry (Izyumov et al., 1991; Wills, 2000; Cui et al., 2006). If the magnetic structure is collinear, which means that the moments in the ordered state point along a unique direction in the structure, then the square of the magnetic structure factor simplifies to

$$|F_{\mathrm{M}}(\boldsymbol{\tau})|^2 = \left\langle 1 - (\hat{\boldsymbol{\tau}}\cdot\hat{\boldsymbol{\eta}})^2 \right\rangle \left| \sum_j \eta_j \left\langle \mu_j^z \right\rangle f_j(\boldsymbol{\tau}) \mathrm{e}^{-W_j}\, \mathrm{e}^{\mathrm{i}\boldsymbol{\tau}\cdot\mathbf{r}_j} \right|^2 \qquad (3)$$

where $\hat{\boldsymbol{\eta}}$ denotes the (common) direction of the ordered moments, η_j denotes the sign of the moment (± 1), $\left\langle \mu_z^j \right\rangle$ is the average value of the ordered moment in thermodynamic equilibrium at (T, H, P, ...), and the orientation factor $\left\langle 1 - (\hat{\boldsymbol{\tau}}\cdot\hat{\boldsymbol{\eta}})^2 \right\rangle$ represents an average over all possible domains. If the magnetic moments are of the same type (e.g., all iron ions that occupy the same crystallographic site in the magnetically disordered phase), then this expression further simplifies to

$$|F_{\mathrm{M}}(\boldsymbol{\tau})|^2 = \left\langle 1 - (\hat{\boldsymbol{\tau}}\cdot\hat{\boldsymbol{\eta}})^2 \right\rangle \langle \mu^z \rangle^2 f^2(\boldsymbol{\tau}) \mathrm{e}^{-2W_j} \left| \sum_j \eta_j\, \mathrm{e}^{\mathrm{i}\boldsymbol{\tau}\cdot\mathbf{r}_j} \right|^2 \qquad (4)$$

Simple examples of this include ferromagnets, or simple $+\ -\ +\ -$ type antiferromagnets. We see from these expressions that neutrons can be used to determine several important quantities: the location of magnetic atoms in the unit cell; the spatial distribution of their magnetic electrons, including possible transfer of net spin onto adjacent sites via bonding; and the dependence of ordered moment $\langle \mu^z \rangle$ on temperature, field, pressure, or other thermodynamic variable, which is direct measure of the order parameter for the phase

transition (e.g., the sublattice magnetization). Often the preferred magnetic axis $\hat{\eta}$ can also be determined from the relative intensities. Finally, the scattering can be put on an absolute scale by internal comparison with the nuclear Bragg intensities I_N from the same sample, given by

$$I_N(\boldsymbol{\tau}) = CM_\tau A(\theta_B)|F_N(\tau)|^2 \tag{5}$$

with

$$|F_N(\boldsymbol{\tau})|^2 = \left|\sum_j b_j \, e^{-W_j} \, e^{i\boldsymbol{\tau}\cdot\mathbf{r}_j}\right|^2 \tag{6}$$

Here b_j is the coherent nuclear scattering amplitude (tabulated for all the elements and isotopes) for the jth atom in the unit cell, and the sum extends over all atoms in the unit cell. Often the nuclear structure is known accurately and F_N can be calculated, or a refinement of the chemical structure can be carried out simultaneously with a refinement of the magnetic structure. In either case the ordered moments on each site can be determined in units of Bohr magnetons.

Subtraction Technique

There are several ways that magnetic Bragg scattering can be distinguished from the nuclear scattering from the structure. Above the magnetic ordering temperature all the Bragg peaks are nuclear in origin, while as the temperature drops below the ordering temperature the intensities of the magnetic Bragg peaks rapidly develop, and for unpolarized neutrons the nuclear and magnetic intensities simply add. If these new Bragg peaks occur at positions that are distinct from the nuclear reflections, then it is straightforward to distinguish magnetic from nuclear scattering. In the case of a ferromagnet, however, or for some antiferromagnets that contain two or more magnetic atoms in the chemical unit cell, these Bragg peaks can occur at the same position. One standard technique for identifying the magnetic Bragg scattering is to make one diffraction measurement in the paramagnetic state well above the ordering temperature and another in the ordered state at the lowest temperature possible, and then subtract the two sets of data. In the paramagnetic state the (free ion) diffuse magnetic scattering is given by (Bacon, 1975)

$$I_{Para} = \frac{2}{3} C \left(\frac{\gamma e^2}{2mc^2}\right)^2 \mu_{eff}^2 f(\mathbf{Q})^2 \tag{7}$$

where μ_{eff} is the effective magnetic moment ($=g[J(J+1)]^{1/2}$ for a free ion). This is a magnetic incoherent cross-section, and the only angular dependence is through the magnetic form factor $f(\mathbf{Q})$. Hence, this scattering looks like "background." There is a sum rule on the magnetic scattering in the system, though, and in the ordered state most of this diffuse scattering shifts into the coherent magnetic Bragg peaks. A subtraction of the high-temperature data (Equation 7) from the data obtained at low temperature (Equation 1) will then yield the magnetic Bragg peaks, on top of a deficit (negative) of scattering away from the Bragg peaks due to the disappearance of the diffuse paramagnetic scattering in the ordered state. This shift in intensity from paramagnetic scattering to Bragg peaks is particularly evident in the diffraction pattern of a polycrystalline sample. On the other hand, all the nuclear cross-sections often do not change significantly with temperature and hence drop out in the subtraction. There are three necessary conditions for this latter assumption to hold and hence the technique to work well. First is that the magnetoelastic interactions are small so that there is no significant change in the crystal structure when the magnetic ordering takes place, second that the Debye–Waller factors in Equation 6 do not differ significantly, and third that the lattice parameters do not have a significant variation with temperature. Here significant means that the peak positions do not change substantially with respect to the instrumental resolution; otherwise the peaks will not be aligned and will need to be adjusted accordingly before subtraction. A related subtraction technique is to apply a large magnetic field in the paramagnetic state to induce a net (ferromagnetic-like) moment. The zero-field (nuclear) diffraction can then be subtracted from the high-field pattern to obtain the intensity associated with the induced moment.

Polarized Beam Technique

When the neutron beam that impinges on a sample has a well-defined polarization state, the nuclear and magnetic scattering that originates from the sample interferes *coherently*, in contrast to being separate cross-sections like Equations 1 and 5 where magnetic and nuclear intensities just add. A simple example is provided by the magnetic and nuclear scattering from elemental iron, which has the body-centered cubic structure and a (saturated) ferromagnetic moment of $2.2\,\mu_B$ at low temperature. It is convenient to define the magnetic scattering amplitude p as (Bacon, 1975)

$$p = \left(\frac{\gamma e^2}{2mc^2}\right)\langle\mu\rangle f(\tau) \tag{8}$$

and then the structure factor for the scattering of polarized neutrons is given by

$$F(\tau) = (b \pm p)e^{-W_j}\left(1 + e^{i\pi(h+k+l)}\right) \tag{9}$$

where "±" indicates the two polarization states of the incident neutrons. The phase factor in parentheses originates from the sum over the unit cell, which in this case is just two identical atoms located at the origin (0, 0, 0) and the body-centered position (1/2, 1/2, 1/2), and (hkl) are Miller indices (unit 1d.1). This gives the familiar selection rule that for a bcc lattice $h + k + l$ must be an even integer for Bragg reflection to occur. The smallest nonzero reciprocal lattice vector is then (1, 1, 0), and for this reflection ($\tau = 3.10\,\text{Å}^{-1}$) the magnetic scattering amplitude is given by

$$p = (0.27 \times 10^{-12}\,\text{cm})(2.2)(0.59) = 0.35 \times 10^{-12}\,\text{cm} \tag{10}$$

The coherent nuclear scattering amplitude for iron is $b = 0.945 \times 10^{-12}$ cm and is independent of the Bragg reflection. The flipping ratio R is defined as the ratio of the intensities for the two neutron polarizations; for this reflection we have

$$R = \left(\frac{0.945 + 0.35}{0.945 - 0.35}\right)^2 = 4.74 \tag{11}$$

Note that for a different Bragg reflection, the only quantity that changes is $f(\boldsymbol{\tau})$, so that a measurement of the flipping ratio at a series of Bragg peaks (hkl) can be used to make precision determinations of the magnetic form factor, and thus by Fourier transform the spatial distribution of the atomic magnetization density. It also should be noted that if $b \approx p$, then the flipping ratio will be very large, and this is in fact one of the standard methods employed to produce a polarized neutron beam in the first place.

In the more general situation when the magnetic structure is not a simple ferromagnet, polarized beam diffraction measurements with polarization analysis of the scattered neutrons must be used to establish unambiguously which peaks are magnetic and which are nuclear, and more generally to separate the magnetic and nuclear scattering at Bragg positions where there are both nuclear and magnetic contributions. The polarization analysis technique as applied to this problem is in principle straightforward; complete details can be found elsewhere (Moon et al., 1969; Williams, 1988). Nuclear coherent Bragg scattering never causes a rotation of the neutron spin direction on scattering, so this scattering never causes a reversal, or spin-flip, of the neutron. Thus, the nuclear peaks will only be observed in the non-spin-flip scattering geometry. We denote this configuration as $(+\ +)$, where the neutron is incident with up spin, and remains in the up state after scattering. Non-spin-flip scattering also occurs if the incident neutron is in the down state, and remains in the down state after scattering (denoted $(-\ -)$). The magnetic cross-sections, on the other hand, depend on the relative orientation of the neutron polarization $\mathbf{P}$ and the reciprocal lattice vector $\boldsymbol{\tau}$. In the configuration where $\mathbf{P} \perp \boldsymbol{\tau}$, typically half the magnetic Bragg scattering involves a reversal of the neutron spin (denoted by $(-\ +)$ or $(+\ -)$), and half does not. Thus, for the case of a purely magnetic reflection the spin-flip $(-\ +)$ and non-spin-flip $(+\ +)$ intensities should be equal in intensity. For the case of a simple collinear magnet where $\mathbf{P} \parallel \boldsymbol{\tau}$, all the magnetic scattering is spin-flip. Hence, for a pure magnetic Bragg reflection the spin-flip scattering should be twice as strong as that for the $\mathbf{P} \perp \boldsymbol{\tau}$ configuration, while ideally no non-spin-flip scattering will be observed. It should be noted that the determination of how much magnetic scattering is spin-flip versus non-spin-flip depends on the detailed nature of the magnetic ions (e.g., whether they behave as Ising, x–y, or Heisenberg moments), but the essential point is that the analysis of these cross-sections can be used to unambiguously identify nuclear from magnetic Bragg scattering.

The arrangement of having $\mathbf{P} \parallel \boldsymbol{\tau}$ or $\mathbf{P} \perp \boldsymbol{\tau}$ provides an experimental simplification and hence data that are straightforward to interpret. More generally, however, $\mathbf{P}$ and $\boldsymbol{\tau}$ can have any relative angle and the magnetic fields in the sample then can rotate the neutron polarization. This more general technique of neutron polarimetry is more difficult to realize experimentally and to interpret the data, but can provide additional details about the magnetic structure that cannot be obtained otherwise (Poole et al., 2009).

Inelastic Scattering

Magnetic inelastic scattering plays a unique role in determining the spin dynamics in magnetic systems, as it is the only probe that can directly measure the complete magnetic excitation spectrum. Typical examples are spin-wave dispersion relations, critical fluctuations, crystal field excitations, and moment/valence fluctuations.

As an example, consider identical spins S on a simple cubic lattice, with a coupling given by $-JS_i \cdot S_j$, where J is the (Heisenberg) exchange interaction between neighbors separated by the distance a. The collective excitations for such a collection of spins are magnons (or loosely termed "spin waves"). If we have $J > 0$ so that the lowest energy configuration is where the spins are parallel (a ferromagnet), then the magnon dispersion along the edge of the cube (the [100] direction) is given by $E(q) = 8JS[\sin^2(qa/2)]$. At each wave vector $\mathbf{q}$, the magnon energy is different, and a neutron can interact with the system of spins and either create a magnon at $(\mathbf{q}, E)$, with a concomitant change of momentum $\mathbf{q}$ and loss of energy E of the neutron, or conversely destroy a magnon with a gain in energy. The observed change in momentum and energy for the neutron can then be used to map out the magnon dispersion relation. Neutron scattering is particularly well suited for such inelastic scattering studies since neutrons typically have energies that are comparable to the energies of excitations in the solid, and therefore the neutron energy changes are large and easily measured. The dispersion relations can then be measured over the entire Brillouin zone (see, e.g., Lovesey, 1984).

Additional information about the nature of the excitations can be obtained by polarized inelastic neutron scattering techniques, which are finding increasing use. Spin-wave scattering is represented by the raising and lowering operators $S^{\pm} = S_x \pm iS_y$, which cause a reversal of the neutron spin when the magnon is created or destroyed. These "spin-flip" cross-sections are denoted by $(+\ -)$ and $(-\ +)$. If the neutron polarization $\mathbf{P}$ is parallel to the momentum transfer $\mathbf{Q}$, $\mathbf{P} \parallel \mathbf{Q}$, then spin angular momentum is conserved (as there is no orbital contribution in this case). In this experimental geometry, we can only create a spin wave in the $(-\ +)$ configuration, which at the same time causes the total magnetization of the sample to decrease by one unit ($1\ \mu_B$). Alternatively, we can destroy a spin wave only in the $(+\ -)$ configuration, while increasing the magnetization by one unit. This gives us a unique way to unambiguously identify the spin-wave scattering,

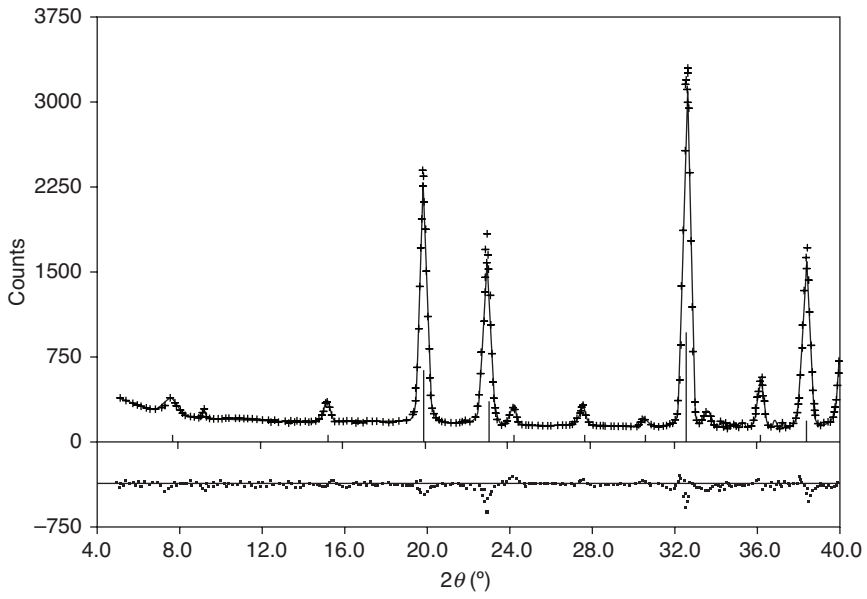

Figure 1. Calculated (solid curve) and observed intensities at room temperature for a powder of antiferromagnetically ordered $YBa_2Fe_3O_8$. The differences between calculated and observed are shown at the bottom (Huang et al., 1992).

and polarized beam techniques in general can be used to distinguish magnetic from nuclear scattering in a manner similar to the case of Bragg scattering.

Finally, we note that the magnetic Bragg scattering is comparable in strength to overall magnetic inelastic scattering. However, all the Bragg scattering is located at a single point in reciprocal space, while the inelastic scattering is distributed throughout the (three-dimensional) Brillouin zone. Hence, when actually making inelastic measurements to determine the dispersion of the excitations, one can only observe a small portion of the dispersion surface at any one time, and thus the observed inelastic scattering is typically two to three orders of magnitude less intense than the Bragg peaks. Consequently, these are much more time-consuming measurements, and larger samples are needed to offset the reduction in intensity. Of course, a successful determination of the dispersion relations yields a complete determination of the fundamental atomic interactions in the solid.

PRACTICAL ASPECTS OF THE METHOD

Diffraction

As an example of Bragg scattering, a portion of the powder diffraction pattern from a sample of $YBa_2Fe_3O_8$ is shown in Figure 1 (Huang et al., 1992). The solid curve is a Rietveld refinement (Young, 1993) of both the antiferromagnetic and crystallographic structures for the sample. From this type of data we can determine the full crystal structure: lattice parameters, atomic positions in the unit cell, site occupancies, etc. We can also determine the magnetic structure and value of the ordered moment. The results of the analysis are shown in Figure 2; the crystal structure is very similar to the structure for the $YBa_2Cu_3O_7$ high-T_C

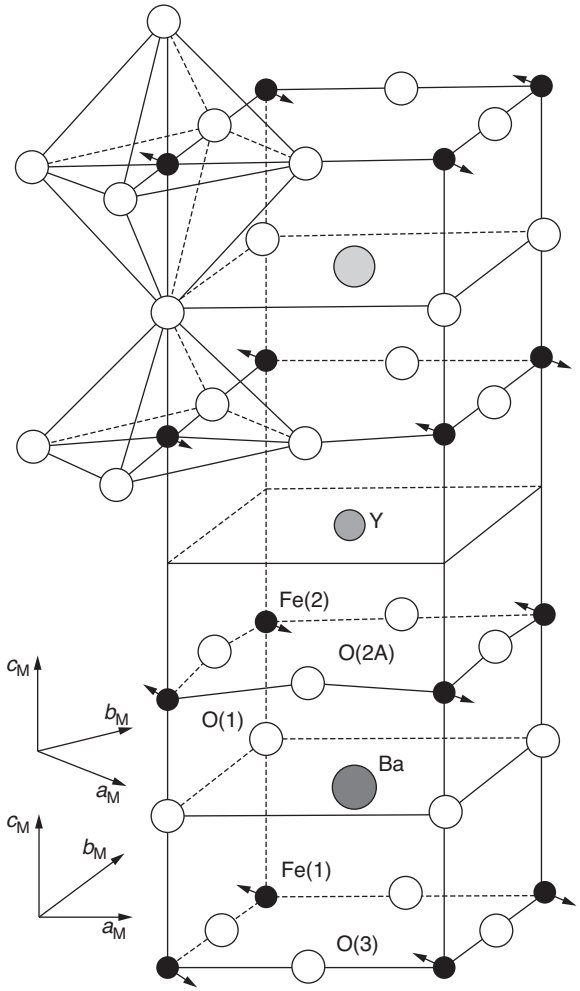

Figure 2. Crystal and magnetic structure for $YBa_2Fe_3O_8$ deduced from the data of Figure 1 (Huang et al., 1992).

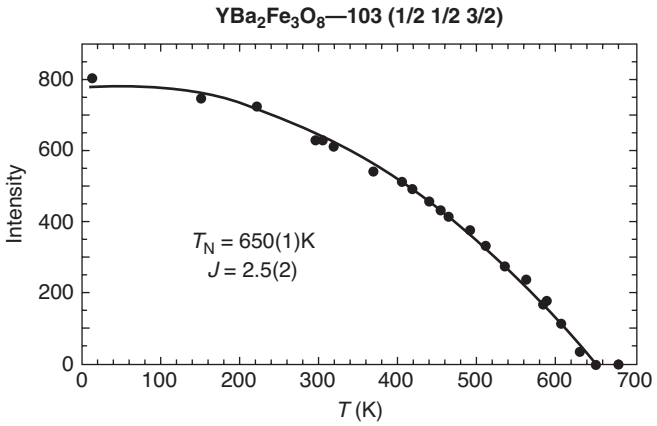

Figure 3. Temperature dependence of the intensity of the magnetic reflection found at a scattering angle of 19.5° in Figure 1. The Néel temperature is 650K (Natali Sora et al., 1994).

cuprate superconductor, with the Fe replacing the Cu, and the magnetic structure is also the same as has been observed for the Cu spins in the oxygen-reduced ($YBa_2Cu_3O_6$) Mott insulator system.

Experimentally we can recognize the magnetic scattering by several characteristics. First, it should be temperature dependent, and the Bragg peaks will vanish above the ordering temperature. Figure 3 shows the temperature dependence of the intensity of the peak at a scattering angle of 19.5° in Figure 1. The data clearly reveal a phase transition at the Néel temperature for $YBa_2Fe_3O_8$ of 650 K (Natali Sora et al., 1994); below the Néel temperature is where long-range antiparallel order of the spins first occurs. Above the antiferromagnetic phase transition this peak completely disappears, indicating that it is a purely magnetic Bragg peak. A second characteristic is that the magnetic intensities become weak at high scattering angles (not shown), as $f(\tau)$ typically falls off strongly with increasing angle. A third, more elegant, technique is to use polarized neutrons. The polarization technique can be used at any temperature, and for any material regardless of whether or not it has a crystallographic distortion (e.g., via magnetoelastic interactions) associated with the magnetic transition. It is more involved and time consuming experimentally, but yields an unambiguous identification and separation of magnetic and nuclear Bragg peaks.

Consider the case of a collinear magnet, and first have $\mathbf{P} \| \tau$, which is generally achieved by having a small (few Oe) horizontal magnetic "guide" field oriented along the scattering vector. In this geometry all the magnetic scattering is spin-flip, while the nuclear scattering is always non-spin-flip. For a magnetic Bragg peak the spin-flip scattering should be twice as strong as for the $\mathbf{P} \perp \tau$ configuration (vertical guide field), while the nuclear scattering is non-spin-flip scattering (and completely independent of the orientation of $\mathbf{P}$ and τ). Figure 4 shows the polarized beam results for the same two peaks, at scattering angles (for this wavelength) of 30° and 35°; these correspond to the peaks at 19.5° and 23° in Figure 1.

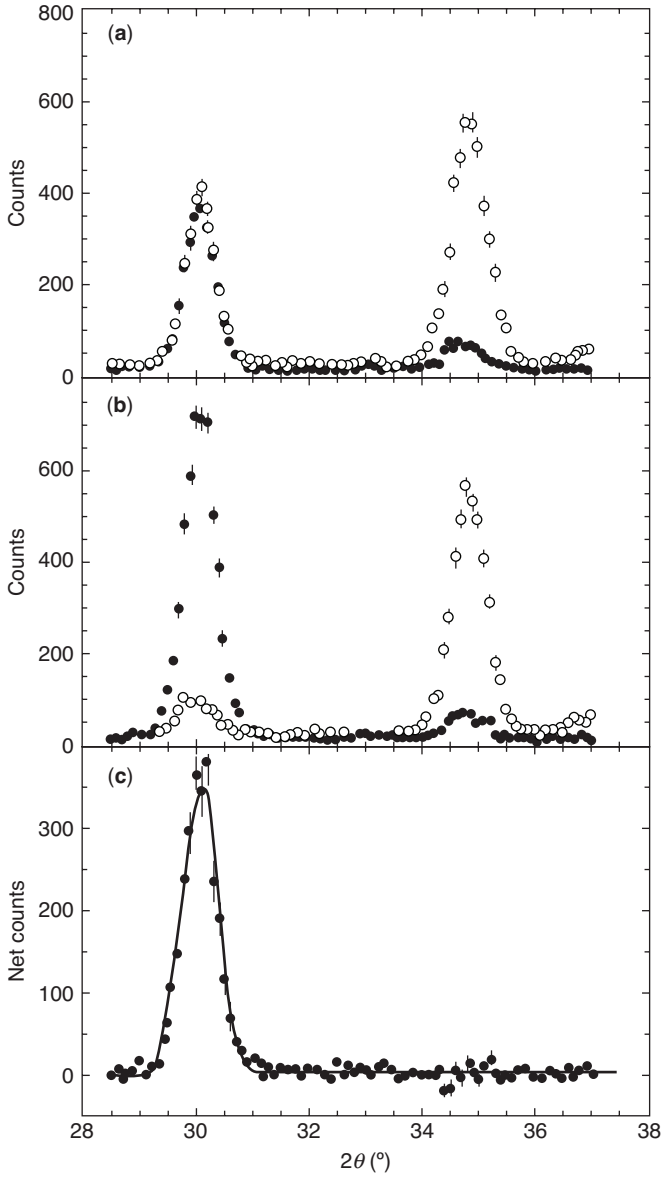

Figure 4. Polarized neutron scattering. The part (**a**) is for $\mathbf{P} \perp \tau$, where the open circles show the non-spin-flip scattering and the filled circles are the observed scattering in the spin-flip configuration. The low angle peak has equal intensity for both cross-sections, and thus is identified as a pure magnetic reflection, while the ratio of the (+ +) to (− +) scattering for the high angle peak is 11, the instrumental flipping ratio. Hence, this is a pure nuclear reflection. The part (**b**) is for $\mathbf{P} \| \tau$, and the part (**c**) is the subtraction of the $\mathbf{P} \perp \tau$ spin-flip scattering from the data for $\mathbf{P} \| \tau$. Note that in this polarized beam subtraction procedure all background and nuclear cross-sections cancel, isolating the magnetic scattering (Huang et al., 1992).

Figure 4a shows the data for the $\mathbf{P} \perp \tau$ configuration. The peak at 30° has the identical intensity for both spin-flip and non-spin-flip scattering, and hence we conclude that this scattering is purely magnetic in origin as inferred from Figure 3. The peak at 35°, on the other hand, has strong intensity for (+ +), while the intensity for (− +) is

smaller by a factor of 1/11, the instrumental flipping ratio in this measurement. Hence, ideally there would be no spin-flip scattering, and this peak is identified as a pure nuclear reflection. Figure 4b shows the same peaks for the $\mathbf{P}||\tau$ configuration, while Figure 4c shows the subtraction of the $\mathbf{P}\perp\tau$ spin-flip scattering from the $\mathbf{P}||\tau$ spin-flip scattering. In this subtraction procedure instrumental background, as well as all nuclear scattering cross-sections, cancels, isolating the magnetic scattering. We see that there is magnetic intensity only for the low angle position, while no intensity survives the subtraction at the 35° peak position. These data unambiguously establish that the 30° peak is purely magnetic, while the 35° peak is purely nuclear. This simple example demonstrates how the technique works; obviously it would play a much more critical role in cases where it is not clear from other means what is the origin of the peaks, such as in regimes where the magnetic and nuclear peaks overlap, or in situations where the magnetic transition is accompanied by a structural distortion. If needed, a complete "magnetic diffraction pattern" can be obtained and analyzed with these polarization techniques.

In cases where there is no significant coupling of the magnetic and lattice systems, on the other hand, the subtraction technique can also be used to obtain the magnetic diffraction pattern (see, e.g., Zhang et al., 1990). This technique is especially useful for low-temperature magnetic phase transitions where the Debye–Waller effects can be safely neglected. Figure 5

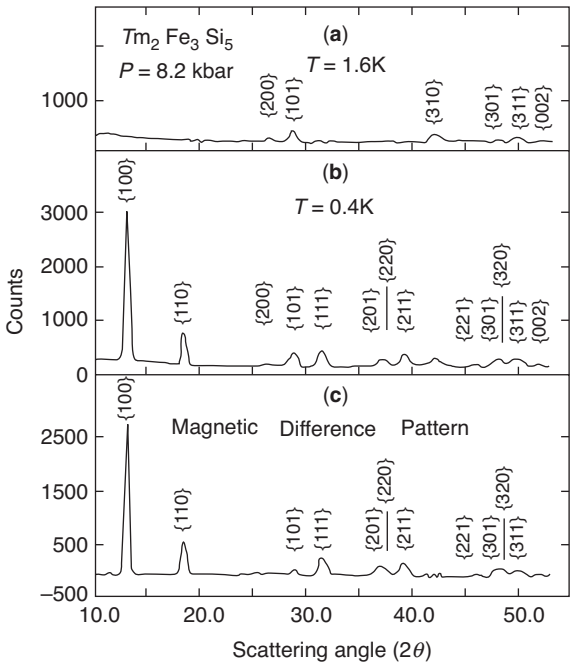

Figure 5. Diffraction patterns with unpolarized neutrons for the antiferromagnetic superconductor $Tm_2Fe_3Si_5$. (**a**) The nuclear diffraction pattern obtained above the antiferromagnetic ordering temperature of 1.1 K, (**b**) the low-temperature diffraction pattern in the ordered state, and (**c**) the subtraction of the parts (**a**) and (**b**), which gives the magnetic diffraction pattern (Gotaas et al., 1987).

shows the diffraction patterns for $Tm_2Fe_3Si_5$, which is an antiferromagnetic material that becomes superconducting under pressure (Gotaas et al., 1987). Figure 5a shows the diffraction pattern obtained above the antiferromagnetic ordering temperature of 1.1 K, where just the nuclear Bragg peaks are observed. Figure 5b shows the low-temperature diffraction pattern in the ordered state, which contains both magnetic and nuclear Bragg peaks, and Figure 5c shows the subtraction, which gives the magnetic diffraction pattern.

The examples above are for polycrystalline samples, and on a new material a good approach is first to measure a polycrystalline sample to determine the basic structure. One evident feature of diffraction from polycrystalline materials is that typically several magnetic peaks will be observed when the scattering is measured over a relatively modest range of diffraction angles, assuming, of course, that the magnetic scattering is strong enough to be observed. Inspection of Equations 1, 3 and 4 shows that the intensity is proportional to the square of the ordered moment(s), and typically it is difficult to observe magnetic peaks when the moment in the polycrystalline sample is $\sim 0.1\ \mu_B$ or less. Regardless of the size of the moment, if suitable single crystals are available, data with much better signal-to-noise can generally be achieved, for all the diffraction quantities of interest. If nothing is known about the magnetic structure, then time-consuming searches, utilizing position-sensitive detectors, will likely be needed to locate the magnetic peaks and determine the nature of the magnetic structure. This is particularly true if the magnetic structure is incommensurate with the underlying crystal structure, such as shown in Figure 6. $ErNi_2B_2C$ becomes superconducting below 11 K and orders magnetically at 6 K into a transversely polarized spin density wave structure, with the modulation wave vector δ along the a axis and the spins collinear along the b direction (or equivalently with δ along b and the spins parallel to the a axis) (Choi et al., 2001). A portion of a scan along the a axis is shown in Figure 6 at three temperatures. Below T_N the initial ordering is into a simple spin density wave as shown in the schematic, with a modulation of $\delta = 0.55a^*$ ($a^* = 2\pi/a$). At $T = 4.58$ K we also observe a third-order peak at $0.35a^*$ [$(2, 0, 0) - 3\delta$]. The data are plotted on a log scale so that at this T the higher-order peak is quite small compared with the fundamental, but its presence indicates that the spin density wave has already begun to square up. At 2.4 K additional higher-order peaks become observable as the magnetic structure continues to square up as indicated schematically in Figure 6b. These peaks are all odd-order harmonics as expected for a square wave where the number of up spins equals the number of down spins (i.e., no net magnetization). The low-T diffraction data ($T = 1.3$ K) indicate that a new series of peaks has developed, which are *even* harmonics of the fundamental wave vector. One possible origin for these new peaks is that the spin density wave couples to the lattice, producing an accompanying charge density wave distortion, but polarized neutron measurements demonstrate that both types of peaks are magnetic in origin. The even-order peaks then demonstrate that a net

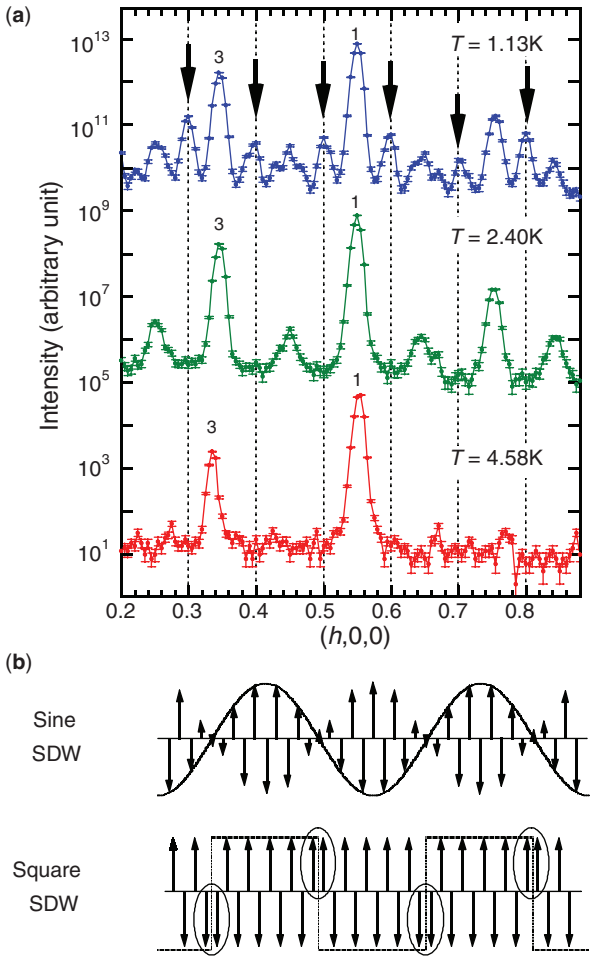

Figure 6. (**a**) Diffraction data along the (h, 0, 0) direction at 1.3, 2.4, and 4.58 K (offset for clarity), plotted on a log scale. Above the weak ferromagnetic transition at 2.3 K there is a fundamental spin density wave peak at $h = 0.55$ along with (weak) odd-order harmonics, while below a new set of even harmonics develops (arrows). (**b**) A schematic of the pure spin density wave

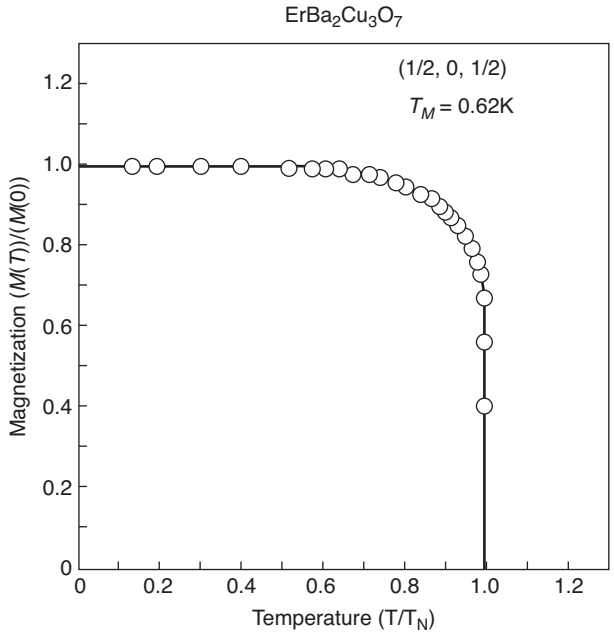

Figure 7. Temperature dependence of the sublattice magnetization for the Er spins in superconducting $ErBa_2Cu_3O_7$, measured on a single crystal weighing 31 mg. The solid curve is Onsager's exact theory for the two-dimensional, $S = {}^1/_2$, Ising model (Lynn et al., 1989).

magnetization has developed in the system, in the superconducting state.

The temperature dependence of the intensity of an antiferromagnetic Bragg peak on a single crystal can be measured quite precisely, and an example is shown in Figure 7 for the Er ordering in the high-T_C superconductor ($T_C \approx 92$ K) $ErBa_2Cu_3O_7$ (Lynn et al., 1989). The magnetic interactions of the Er moments in this material are highly anisotropic, and this system turns out to behave as an ideal two-dimensional (planar) Ising antiferromagnet. The solid curve is Onsager's (1944) exact solution to the $S = {}^1/_2$, two-dimensional Ising model, and we see that it provides an excellent representation of the experimental data.

An example where both structural and magnetic phase transitions occur in close proximity is provided by $SrFe_2As_2$ (Zhao et al., 2008), one of the "parent" materials of the iron-based superconductor family (Lynn and Dai, 2009). A structural distortion from tetragonal to orthorhombic symmetry occurs almost simultaneously with the development of long-range commensurate antiferromagnetic order. Figure 8a shows the temperature evolution of the (2, 2, 0) tetragonal peak, which abruptly splits into the (4, 0, 0) and (0, 4, 0) orthorhombic peaks below 220(1)K. The observation of both (4, 0, 0) and (0, 4, 0) peaks indicates that this single crystal has equally populated twin domains after transforming into the orthorhombic phase. Figure 8b compares the structural phase transition and magnetic order parameter in detail as a function of temperature. It is evident that the structural transition occurs quite abruptly compared to the magnetic phase transition. By normalizing magnetic peaks to the nuclear peaks, a ground-state ordered iron moment of 0.94(4) μ_B was determined. Note that for neutron scattering typically numbers in parentheses and error bars in figures indicate one standard deviation statistical uncertainty.

For epitaxial thin films and multilayers the basic diffraction technique is the same as for bulk single crystals. However, because of the small amount of material contained in the film (and usually a much larger substrate), the measurements are more challenging. The final diffraction example is shown in Figure 9 for two Fe_3O_4/CoO superlattices (Ijiri et al., 1998). The superlattices consist of 50 repeats of 100 Å thick layers of magnetite, which is a ferrimagnet, and either 30 or 100 Å thick layers of the antiferromagnet CoO. The superlattices were grown epitaxially on single crystal MgO substrates, and thus these may be regarded as single crystal samples. These scans are along the growth direction (Q_z), and show the changes in the magnetic

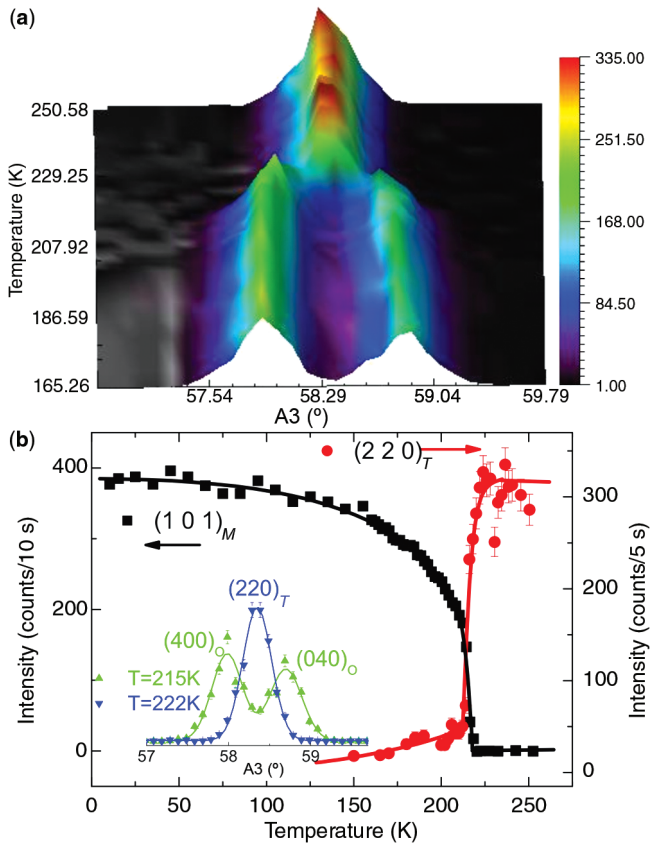

Figure 8. Structural and magnetic phase transition as a function of temperature in a single crystal of $SrFe_2As_2$. (**a**) Temperature dependence of the $(2, 2, 0)_T$ structural peak, showing that it abruptly splits below 220 K. (**b**) Comparison of the structural distortion and magnetic order parameter, both occurring at essentially the same temperature. The structural transition is abrupt, while the magnetic transition appears to be (nearly) continuous (Zhao et al., 2008).

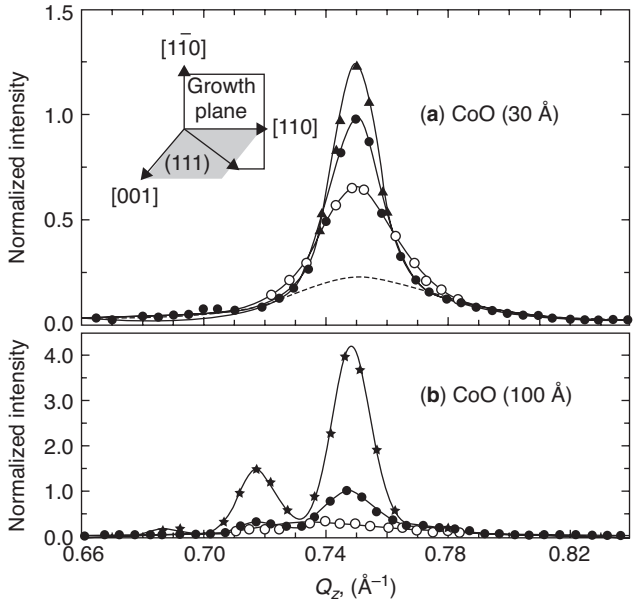

Figure 9. Neutron diffraction scans of the (111) reflection along the [001] growth axis direction (scattering vector Q_z) for (**a**) $[Fe_3O_4$ (100 Å)/CoO(30 Å)$]_{50}$ and (**b**) $[Fe_3O_4$ (100 Å)/CoO(100 Å)$]_{50}$ superlattices, taken at 78 K in zero applied field. (•) Data taken after zero-field cooling (initial state), (°) field cooling with an applied field ($H = 1.4$ T) in the [1$\bar{1}$0] direction, and (Δ) field cooling with an applied field in the [110] direction, respectively. The inset illustrates the scattering geometry. The dashed lines indicate the temperature- and field-independent Fe_3O_4 component (Ijiri et al., 1998).

scattering that occur when the sample is cooled in an applied field versus zero-field cooling. These data, together with polarized beam data taken on the same samples, have elucidated the origin of the technologically important exchange biasing effect that occurs in these magnetic superlattices.

It is interesting to compare the type and quality of data that are represented by these examples. The powder diffraction technique is quite straightforward, to both obtain and analyze the data. In this case typical sample sizes are $\sim 1 \rightarrow 20$ g, and important and detailed information can be readily obtained with such sample sizes in a few hours of spectrometer time, depending on the particulars of the problem. The temperature dependence of the order parameter in $ErBa_2Cu_3O_7$, on the other hand, was obtained on a single crystal weighing only 31 mg. Note that the statistical quality of the data is much better than for the powder sample even though the sample is more than two orders of magnitude smaller; this is because it is a single crystal and all the scattering is directed into a single Bragg peak, rather than scattering into a powder diffraction ring. The final example was for Fe_3O_4/CoO superlattices, where the weight of the superlattices that contributes to the scattering is approximately 1 mg. Thus, it is clear that interesting and successful diffraction experiments can be carried out on quite small samples.

The final example in this section addresses the measurement of a magnetic form factor, in the cubic antiferromagnetic K_2IrCl_6. The Ir ions occupy a face-centered cubic lattice, and the 5d electrons carry a magnetic moment that is covalently bonded to the six Cl ions located octahedrally around each Ir ion. One of the interesting properties of this system is that there is charge transfer from the Ir equally onto the six Cl ions. A net spin transfer, however, only occurs for the two Cl ions along the direction in which the Ir spin points. This separation of spin and charge degrees of freedom leads to a very unusual form factor that is highly anisotropic, as shown in Figure 10 (Lynn et al., 1976). Note the rapid decrease in the form factor as one proceeds along the spin direction (the c axis), from the $(0, 1, \frac{1}{2})$ to the $(0, 1, \frac{3}{2})$, and then to the $(0, 1, \frac{5}{2})$ Bragg peak, which in fact has an unobservable intensity. In this example, approximately 30% of the total moment is transferred onto the Cl ions, which is why these covalency effects are so large in this compound. It should be noted that, in principle, x-ray scattering should be able to detect the charge

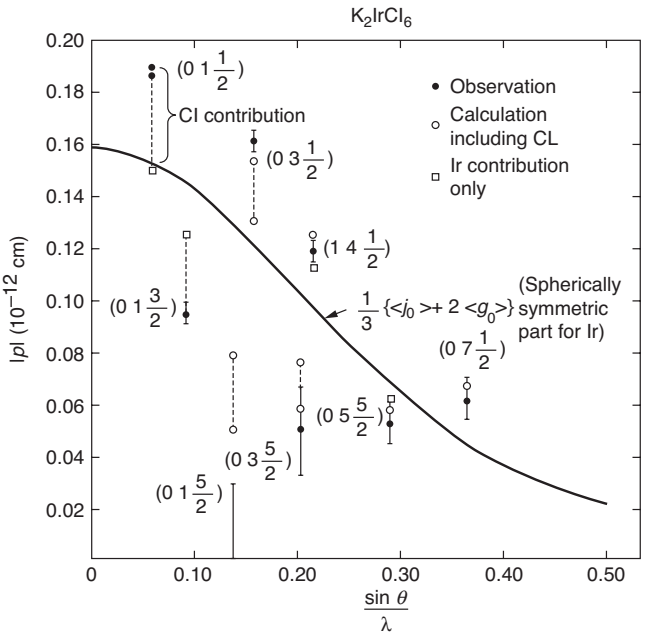

Figure 10. Comparison of the observed and calculated magnetic form factor for the cubic K_2IrCl_6 system, showing the enormous directional anisotropy along the spin direction ([00*l*] direction) compared with perpendicular to the spin direction. The contribution of the Cl moments along the spin direction, arising from the covalent bonding, is also indicated; no net moment is transferred to the Cl ions that are perpendicular to the spin direction (Lynn et al., 1976).

transferred onto the (six) Cl ions as well, but this is much more difficult to observe because it is a very small fraction of the total charge. In the magnetic case, in contrast, it is a large percentage effect and has a different symmetry than the lattice, which makes the covalent effects much easier to observe and interpret.

Inelastic Scattering

There are many types of magnetic excitations and fluctuations that can be measured with neutron scattering techniques, such as magnons, critical fluctuations, crystal field excitations, magnetic excitons, and moment/valence fluctuations. To illustrate the basic technique, consider an isotropic ferromagnet at sufficiently long wavelengths (small q). The spin-wave dispersion relation is given by $E_{sw} = D(T)q^2$, where D is the spin-wave "stiffness" constant. The general form of the spin-wave dispersion relation is the same for all isotropic ferromagnets, a requirement of the (assumed) perfect rotational symmetry of the magnetic system, while the numerical value of D depends on the details of the magnetic interactions and the nature of the magnetism. One example of a prototypical isotropic ferromagnet is amorphous $Fe_{86}B_{14}$. Figure 11 shows an example of polarized beam inelastic neutron scattering data taken on this system (Lynn et al., 1993). These data were taken with the neutron polarization $\mathbf{P}$ parallel to the momentum transfer $\mathbf{Q}$ ($\mathbf{P} \| \mathbf{Q}$), where we should be able to create

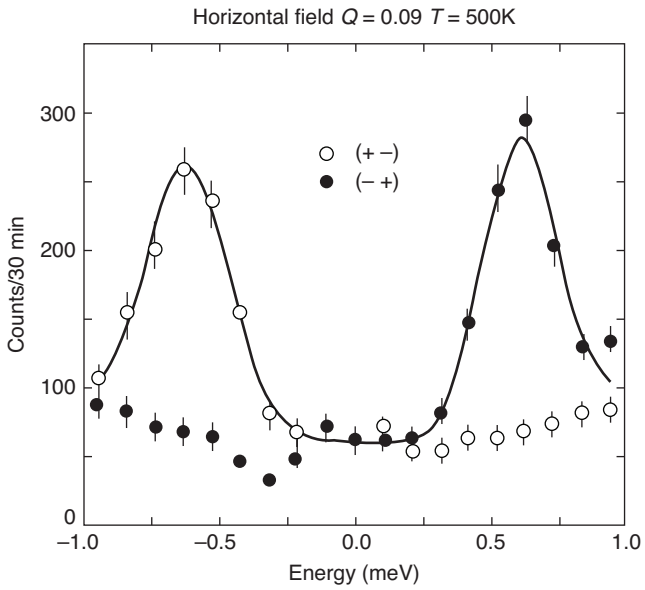

Figure 11. Spin-flip scattering observed for the amorphous Invar $Fe_{86}B_{14}$ isotropic ferromagnetic system in the $\mathbf{P} \| \mathbf{Q}$ configuration. Spin waves are observed for neutron energy gain ($E < 0$) in the (+ −) cross-section, and for neutron energy loss ($E > 0$) in the (− +) configuration (Lynn et al., 1993).

a spin wave only in the (− +) configuration, or destroy a spin wave only in the (+ −) configuration. This is precisely what we see in the data; for the (− +) configuration the spin waves can only be observed for neutron energy loss scattering ($E > 0$), while for the (+ −) configuration spin waves can only be observed in neutron energy gain ($E < 0$). This behavior of the scattering uniquely identifies these excitations as spin waves.

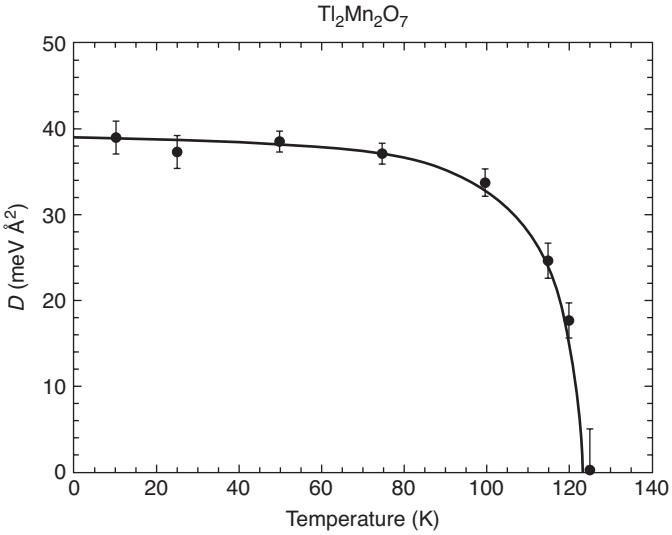

Figure 12. Temperature dependence of the spin-wave stiffness $D(T)$ in the magnetoresistive $Tl_2Mn_2O_7$ pyrochlore, showing that the spin waves renormalize as the ferromagnetic transition is approached (Lynn et al., 1998). Below T_C the material is a metal, while above T_C it exhibits insulator behavior.

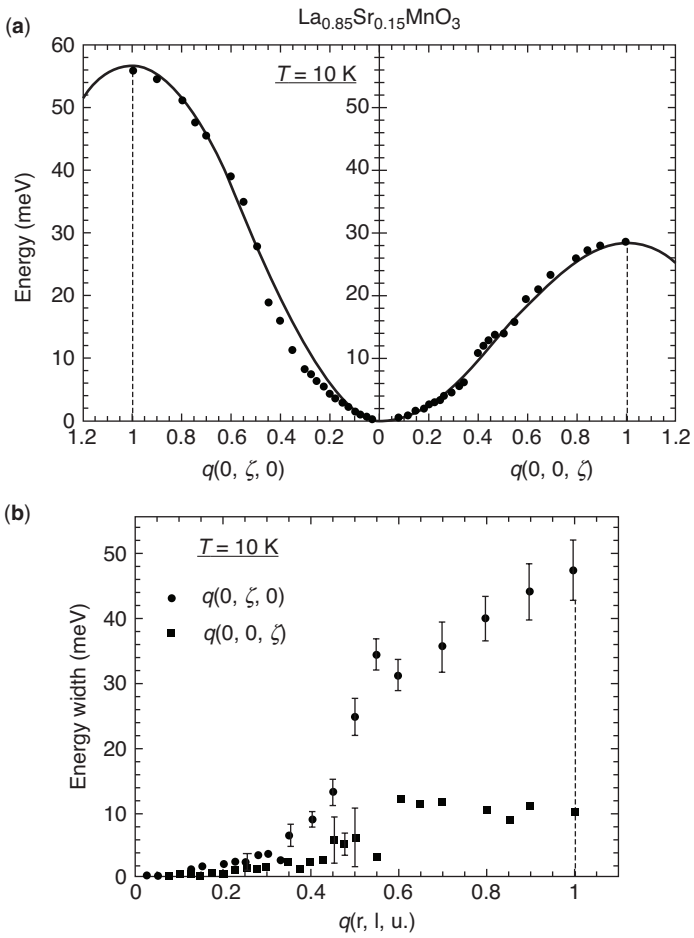

Figure 13. (**a**) Ground-state spin-wave dispersion along the (0, 1, 0) and (0, 0, 1) directions measured to the zone boundary for the magnetoresistive manganite $La_{0.85}Sr_{0.15}MnO_3$. The solid curves are a fit to the dispersion relation for a simple Heisenberg exchange model. (**b**) The intrinsic linewidths of the excitations. In the standard models, intrinsic linewidths are expected only at elevated temperatures. The large observed linewidths demonstrate the qualitative inadequacies of these models (Vasiliu-Doloc et al., 1998).

Data like these can be used to measure the renormalization of the spin waves as a function of temperature, as well as determine the lifetimes as a function of wave vector and temperature. An example of the renormalization of the "stiffness" constant D for the magnetoresistive oxide $Tl_2Mn_2O_7$ is shown in Figure 12 (Lynn et al., 1998). Here the wave vector dependence of the dispersion relation has been determined at a series of q, and the stiffness parameter extracted from the data. The variation in the stiffness parameter is then plotted, and indicates a smooth variation with a ferromagnetic transition temperature of 123 K. These measurements can then be compared directly with theoretical calculations. They can also be compared with other experimental observations, such as magnetization measurements, whose variation with temperature originates from spin-wave excitations.

Finally, these types of measurements can be extended all the way to the zone boundary on single crystals. Figure 13 shows an example of the spin-wave dispersion relation for the ferromagnet $La_{0.85}Sr_{0.15}MnO_3$, a system that undergoes a metal–insulator transition that is associated with the transition to ferromagnetic order (Vasiliu-Doloc et al., 1998). Figure 13a shows the dispersion relation for the spin-wave energy along two high-symmetry directions, and the solid curves are fits to a simple nearest-neighbor spin-coupling model. The overall trend of the data is in reasonable agreement with the model, although there are some clear discrepancies as well, indicating that a more sophisticated model is needed in order to obtain quantitative agreement. In addition to the spin-wave energies, though, information about the intrinsic lifetimes can also be determined, and these linewidths are shown in Figure 13b for both symmetry directions. In the simplest type of model, no intrinsic spin-wave linewidths at all would be expected at low temperatures, while we see here that the observed linewidths are very large and highly anisotropic, indicating that an itinerant electron type of model is more appropriate for this system.

METHOD AUTOMATION

Neutrons for materials research are produced by one of the following two processes: fission of U^{235} in a nuclear reactor and the spallation process where high-energy protons from an accelerator impact on a heavy metal target such as tungsten or liquid mercury and burst the nuclei. Both techniques produce high-energy (MeV) neutrons, which are then thermalized or subthermalized in a moderator (such as heavy water) to produce a Maxwellian spectrum of thermal or cold neutrons, with energies in the meV range. Thus, all neutron scattering instrumentation is located at centralized facilities, and each facility generally has a wide variety of instrumentation that has been designed and constructed for the specific facility, and is maintained and scheduled by facility scientists. Generally any of these instruments can be used to observe magnetic scattering, and with the number and diversity of spectrometers in operation it is not practical to review the instrumentation here; the interested user should contact one of the facilities directly. The facilities themselves operate for periods of weeks at a time continuously, and hence since the early days of neutron scattering all the data collection has been accomplished by automated computer control.

SAMPLE PREPARATION

As a general rule there is no particular preparation that is required for the sample, in the sense that there is no need, for example, to polish the surface, cleave it under high vacuum, or similar procedures. Neutrons are a deeply penetrating bulk probe, and hence generally do not interact with the surface. There are two exceptions to this rule. One is when utilizing polarized neutrons in the investigation of systems with a net magnetization, where a rough surface can cause the variations in the local

magnetic field that depolarize the neutrons. In such cases the surface may need to be polished. The second case is for neutron reflectometry, where small-angle mirror reflection is used to directly explore the magnetization profile of the surface and interfacial layers. In this case the samples need to be optically flat over the full size of the sample (typically 1–10 cm^2), and, of course, the quality of the film in terms of surface roughness, epitaxial quality, etc., becomes part of the investigation.

For magnetic single crystal diffraction, typical sample sizes should be no more than a few cubic millimeters in order to avoid primary and secondary extinction effects; if the sample is too large, extinction will always limit the accuracy of the data obtained. Since the magnetic Bragg intensity is proportional to the square of the ordered moment, any extinction effects will depend on the value of $\langle \mu_z \rangle$ at a particular temperature and field, while the ideal size of the sample can vary by three to four orders of magnitude depending on the value of the saturation moment.

Powder diffraction requires gram-sized samples, generally in the range of 1–20 g. The statistical quality of the data that can be obtained is directly related to the size, so in principle there is a direct trade-off between sample size and the time required to collect a set of diffraction data at a particular temperature or magnetic field. Sample sizes smaller than 1 g can certainly be measured but this translates into fewer data sets, so an adequate-sized sample is highly desirable.

The cross-sections for inelastic scattering are typically two to three orders of magnitude smaller than elastic cross-sections, and therefore crystals for inelastic scattering typically must be correspondingly larger in comparison with single crystal diffraction. Consequently, for both powder diffraction and inelastic scattering the general rule is the following: the bigger the sample, the better the data. The exception is if one or more of the elements in a material has a substantial nuclear absorption cross-section, in which case the optimal size of the sample is then determined by the inverse of this absorption length. The absorption cross-sections are generally directly proportional to the wavelength of the neutrons being employed for a particular measurement, and the optimal sample size then depends on the details of the spectrometer and the neutron wavelength(s). The absorption cross-sections for all the elements can be found in Section "Internet Resources." In some cases particular isotopes can be substituted to avoid some large absorption cross-sections, but generally these are expensive and/or are only available in limited quantity. Therefore, isotopic substitution can be employed only for a few isotopes that are relatively inexpensive, such as deuterium or boron, or in scientifically compelling cases where the cost can be justified.

DATA ANALYSIS AND INITIAL INTERPRETATION

One of the powers of neutron scattering is that it is a very versatile tool and can be used to probe a wide variety of magnetic systems over enormous ranges of length scale ($\sim$0.1–10,000 Å) and dynamic energy ($\sim$10 neV to 1 eV). The instrumentation to provide these measurement capabilities is equally diverse, but data analysis software is generally provided for each instrument to perform the initial interpretation of the data. Moreover, the technique is usually sufficiently fundamental and the interpretation sufficiently straightforward that the initial data analysis is often all that is needed.

PROBLEMS

Neutron scattering is a very powerful technique, but in general it is flux limited, and this usually requires a careful trade-off between instrumental resolution and signal. There can also be unwanted cross-sections that appear and contaminate the data, and so one must, of course, exercise care in collecting the data and be vigilant in its interpretation. If a time-of-flight spectrometer is being employed, for example, there may be frame overlap problems that can mix the fastest neutrons with the slowest, and give potentially spurious results. Similarly, if the spectrometer employs one or more single crystals to monochromate or analyze the neutron energies, then the crystal can reflect higher-order wavelengths (since Bragg's law is $n\lambda = 2d\sin(\theta)$) that can give spurious peaks. Sometimes these can be suppressed with the use of filters or velocity selectors, but more generally it is necessary to vary the spectrometer conditions and retake the data in order to identify genuine cross-sections from spurious ones. This identification process can consume considerable beam time.

Another problem can be encountered in identifying the magnetic Bragg scattering in powders using the subtraction technique. If the temperature is sufficiently low, the nuclear spins may begin to align with the electronic spins, particularly if there is a large hyperfine field. Significant polarization can occur at temperatures of a few degrees Kelvin and lower, and the nuclear polarization can be confused with electronic magnetic ordering. Another problem can be encountered if the temperature dependence of the Debye–Waller factor is significant, or if there is a structural distortion associated with the magnetic transition such as through a magnetoelastic interaction. In this case the nuclear intensities would not be identical and thus they would not cancel correctly in the subtraction. It is up to the experimenter to decide if this is a problem, within the statistical precision of the data. A problem can also occur if there is a significant thermal expansion, where the diffraction peaks shift position with temperature. By significant we mean that the shift is noticeable in comparison with the instrumental resolution employed. Again it is up to the experimenter to decide if this is a problem. In both these latter cases, though, a full refinement of the combined magnetic and nuclear structures in the ordered phase can be carried out. Alternatively, polarized beam techniques can be employed to unambiguously separate the magnetic and nuclear cross-sections. Finally, if one uses the subtraction technique in the method where a field is applied, the field can cause the powder particles to reorient if there is substantial crystalline magnetic anisotropy in the sample. This

preferred orientation will remain when the field is removed and will be evident in the nuclear peak intensities, but must be taken into account.

Finally, we remark about the use of polarized neutrons. Highly polarized neutron beams can be produced by single crystal diffraction from a few special magnetic materials, from magnetic mirrors, or from transmission of the beam through a few specific nuclei where the absorption cross-section is strongly spin dependent. The choices are limited, and consequently most spectrometers are not equipped with polarization capability. For instruments that do have a polarized beam option, generally one has to sacrifice instrumental performance in terms of both resolution and intensity. Polarization techniques are then typically not used for many problems in a routine manner, but rather are usually used to answer some specific question or make an unambiguous identification of a cross-section, most often after measurements have already been carried out with unpolarized neutrons.

ACKNOWLEDGMENTS

I would like to thank my colleagues, Julie Borchers, Qing Huang, Yumi Ijiri, Nick Rosov, Tony Santoro, and Lida Vasiliu-Doloc, for their assistance in the preparation of the original tutorial and update.

There are vast numbers of studies in the literature on the various aspects presented here. The specific illustrative examples used here were chosen for their tutorial value, but also for the author's convenience in obtaining the figures and familiarity with the work.

BIBLIOGRAPHY

"Magnetic Neutron Scattering" in *Characterization of Materials*, 1st ed., Vol. 2, pp. 1328–1339, by J. W. Lynn, University of Maryland, College Park, Maryland.

LITERATURE CITED

Bacon, G. E. 1975. Neutron Diffraction, 3rd ed. Oxford University Press, Oxford.

Blume, M. 1961. Orbital contribution to the magnetic form factor of Ni^{++}. *Phys. Rev.* 124:96–103.

Choi, S. M., Lynn, J. W., Lopez, D., Gammel, P. L., Canfield, P. C., and Bud'ko, S. L. 2001. Direct observation of spontaneous weak-ferromagnetism in the superconductor $ErNi_2B_2C$. *Phys. Rev. Lett.* 87: 107001, 1–4.

Cui, J., Huang, Q., and Toby, B. H. 2006. Magnetic structure refinement with neutron powder diffraction data using GSAS: A tutorial. *Powder Diffraction* 21:71–79.

Gotaas, J. A., Lynn, J. W., Shelton, R. N., Klavins, P., and Braun, H. F. 1987. Suppression of the superconductivity by antiferromagnetism in $Tm_2Fe_3Si_5$. *Phys. Rev. B* 36:7277–7280.

Huang, Q., Karen, P., Karen, V. L., Kjekshus, A., Lynn, J. W., Mighell, A. D., Rosov, N., and Santoro, A. 1992. Neutron powder diffraction study of the nuclear and magnetic structures of $YBa_2Cu_3O_8$. *Phys. Rev. B* 45:9611–9619.

Ijiri, Y., Borchers, J. A., Erwin, R. W., Lee, S.-H., van der Zaag, P. J., and Wolf, R. M. 1998. Perpendicular coupling in exchange-biased Fe_3O_4/CoO superlattices. *Phys. Rev. Lett.* 80:608–611.

Izyumov, Yu. A., Naish, V. E., and Ozerov, R. P. 1991. Neutron Diffraction of Magnetic Materials. Consultants Bureau, New York. (translated from Russian by Joachim Büchner).

Lovesey, S. W. 1984. Theory of Neutron Scattering from Condensed Matter, Vol. 2 Oxford, New York.

Lynn, J. W. and Dai, P. 2009. Neutron studies of the iron-based family of high Tc magnetic superconductors. *Physica C* 469:469–476.

Lynn, J. W., Clinton, T. W., Li, W-H., Erwin, R. W., Liu, J. Z., Vandervoort, K., and Shelton, R. N. 1989. *Phys. Rev. Lett.* 63:2606–2610.

Lynn, J. W., Rosov, N., and Fish, G. 1993. Polarization analysis of the magnetic excitations in Invar and non-Invar amorphous ferromagnets. *J. Appl. Phys.* 73:5369–5371.

Lynn, J. W., Shirane, G., and Blume, M. 1976. Covalency effects in the magnetic form factor of Ir in K_2IrCl_6. *Phys. Rev. Lett.* 37:154–157.

Lynn, J. W., Vasiliu-Doloc, L., and Subramanian, M. 1998. Spin dynamics of the magnetoresistive pyrochlore $Tl_2Mn_2O_7$. *Phys. Rev. Lett.* 80:4582–4586.

Moon, R. M., Riste, T., and Koehler, W. C. 1969. Polarization analysis of thermal neutron scattering. *Phys. Rev.* 181:920–931.

Natali Sora, I., Huang, Q., Lynn, J. W., Rosov, N., Karen, P., Kjekshus, A., Karen, V. L., Mighell, A. D., and Santoro, A. 1994. Neutron powder diffraction study of the nuclear and magnetic structures of the substitutional compounds $(Y_{1-x}Ca_x)Ba_2Fe_3O_{8+\delta}$. *Phys. Rev. B* 49:3465–3472.

Poole, A., Lelievre-Berna, E., and Wills, A. S. 2009. General refinement strategy for magnetic structures using spherical neutron polarimetry and representation analysis. *Physica B* 404:2535–2538.

Trammell, G. T. 1953. Magnetic scattering of neutrons from rare earth ions. *Phys. Rev.* 92:1387–1393.

Vasiliu-Doloc, L., Lynn, J. W., Moudden, A. H., de Leon-Guevara, A. M., and Revcolevschi, A. 1998. Structure and spin dynamics of $La_{0.85}Sr_{0.15}MnO_3$. *Phys. Rev. B* 58:14913–14921.

Williams, G. W. 1988. Polarized Neutrons. Oxford, New York.

Wills, A. S. 2000. A new protocol for the determination of magnetic structures using simulated annealing and representational analysis—SARAh. *Physica B* 276:680–681.

Young, R. A. 1993. The Rietveld Method. Oxford University Press, Oxford.

Zhang, H., Lynn, J. W., Li, W.-H., Clinton, T. W., and Morris, D. E. 1990. Two- and three-dimensional magnetic order of the rare earth ions in $RBa_2Cu_4O_8$. *Phys. Rev. B* 41:11229–11236.

Zhao, J., Ratcliff, II, W., Lynn, J. W., Chen, G. F., Luo, J. L., Wang, N. L., Hu, J., and Dai, P. 2008. Spin and lattice structure of single crystal $SrFe_2As_2$. *Phys. Rev. B* 78: 140504(R), 1–4.

KEY REFERENCES

Bacon, 1975. See above.

This text is more for the experimentalist, treating experimental procedures and the practicalities of taking and analyzing data. It does not contain some of the newest techniques, but has most of the fundamentals. It is also rich in the history of many of the techniques.

Balcar, E., and Lovesey, S. W. 1989. Theory of Magnetic Neutron and Photon Scattering. Oxford, New York. *More recent work that specifically addresses the theory for the case of magnetic neutron as well as x-ray scattering.*

Furrer, A., Mesot, J., and Strässle, T. 2009. Neutron Scattering in Condensed Matter Physics. World Scientific, New Jersey. *Provides an excellent introduction to neutron scattering techniques as they are applied to hard condensed matter physics and materials research.*

Lovesey, 1984. See above.

This text treats the theory of magnetic neutron scattering in depth. Vol. 1 covers nuclear scattering.

Moon et al., 1969. See above.

This is the classic article that describes the triple-axis polarized beam technique, with examples of all the fundamental measurements that can be made with polarized neutrons. Very readable.

Price, D. L. and Sköld, K. 1987. Methods of Experimental Physics: Neutron Scattering. Academic Press, Orlando. *A recent compendium that covers a variety of topics in neutron scattering, in the form of chapters by various experts.*

Squires, G. L. 1978. Thermal Neutron Scattering. Cambridge, New York. *This book is more of a graduate introductory text to the subject of neutron scattering.*

Williams, 1988. See above.

This textbook focuses on the use of polarized neutrons, with all the details.

Young, 1993. See above.

This text details the profile refinement technique for powder diffraction.

INTERNET RESOURCES

Magnetic Form Factors

Numerical values of the free-ion magnetic form factors can be obtained at https://www.ill.eu/sites/ccsl/ffacts/ffachtml.html.

Nuclear Scattering Amplitudes

Values of the coherent nuclear scattering amplitudes and other nuclear cross-sections can be found at http://www.ncnr.nist.gov/resources/n-lengths/.